

Massive vortices in a binary mixture of Bose-Einstein condensates

Andrea Richaud* and Vittorio Penna

*Dipartimento di Scienza Applicata e Tecnologia and u.d.r. CNISM,
Politecnico di Torino, Corso Duca degli Abruzzi 24, I-10129 Torino, Italy*

Montserrat Guilleumas and Ricardo Mayol

*Departament de Física Quàntica i Astrofísica and Institut de Ciències del Cosmos,
Facultat de Física, Universitat de Barcelona, E-08028 Barcelona, Spain*

(Dated: November 23, 2022)

We thoroughly analyze a notable class of states peculiar to a bosonic repulsive binary mixture loaded in a rotating box-like circular trap, i.e. states where vortices in one species host the atoms of the other species, which thus play the role of massive cores. Within a fully-analytic framework, we calculate the equilibrium distance distinguishing the motion of precession of two corotating massive vortices, the angular momentum of each condensed species, the vortices healing length and the cores characteristic size. We then compare these previsions with the measures extracted from the numerical solutions of the associated coupled Gross-Pitaevskii equations. Interestingly, making use of a suitable change of reference frame, we show that the vortices drag the massive cores which they host thus conveying them their same motion of precession, but there is no evidence of quantum viscous friction between the two fluids, since the cores keep their orientation constant while orbiting.

I. INTRODUCTION

Vortices in quantum fluids are topological excitations characterized by quantized circulation [1] which are present in a number of nonlinear field theories and models [2], ranging from superfluid media [3, 4] and quantum optics [5, 6] to superconductivity theories [7, 8] and Josephson-junction arrays [9, 10] and play a key-role in fundamental effects such as superfluid turbulence [11], the Berezinskii-Kosterlitz-Thouless transition [12], fractional statistics [13], and in the development of a fully quantized field theory for topologically complex excitations [14–16]. Among the plethora of different physical systems where vortices can be experimentally investigated, ultracold quantum gases provide a particularly controllable and versatile platform [17, 18] for the study and the observation of the rich phenomenology associated to their formation [19, 20], dynamics [21, 22], and interactions [23]. Vortices in Bose-Einstein condensates (BECs) were first obtained by means of a phase-imprinting method involving two hyperfine spin states of ^{87}Rb [24] but, at present, can be produced also by stirring the BEC above a certain critical velocity [25–27], dragging barriers through the BEC itself [28] or interfering multiple condensate fragments [29].

Solitons are a kind of localized excitations which, because of the competition between dispersion and nonlinearity, propagate keeping their shape unaltered, even if a two-soliton collision occurs [30]. Soon after the achievement of Bose-Einstein condensation, different types of solitons have been described and observed [18, 31, 32]. To our purposes, of particular importance are those systems where a bosonic binary mixture features dark-bright

soliton configurations [33–35]. These structures, first predicted in Ref. [36], are frequently termed as “symbiotic solitons” [37] because the bright component, being endowed with repulsive intraspecies interaction, could not exist if the dark component did not play the role of an effective confining potential.

The same symbiotic relationship was shown to constitute the mechanism underlying the robustness of vortex-bright soliton complexes [38], the topological extension of the dark-bright soliton configuration to the case where a component hosts one or more vortices. The aforementioned study paved the way to a series of further investigations which highlighted, among various aspects, the spontaneous generation of vortex-bright soliton structures [39], the possibility, for the effective potential well corresponding to the vortex core, to support not only the fundamental state, but also multi-ring excited radial state complexes [40], and a rich dynamical scenario for the bright-solitary component [41].

Within an analytical framework and by means of extensive numerical simulations, our work aims at thoroughly analyzing the static and the dynamical properties of vortex-bright soliton complexes, i.e. how the presence of massive solitons within the cores of two corotating vortices affect the equilibrium distance characterizing their motion of precession around the trap center, the role of the interspecies repulsion as an antagonist to the centrifugal force acting on the solitons, the functional dependence of the angular momenta carried by two species, of the vortex healing lengths, and of the cores’ characteristic radius on the mass of the cores.

If one considers repulsive intra- and interspecies interactions such that, in the homogeneous case, the system would be demixed, the dynamical picture of the mixture [in which the order-parameter fields of the two species obey two coupled Gross-Pitaevskii equations (GPEs)], indeed reduces to the much simpler equations of two point-

* Correspondence to: andrea.richaud@polito.it

like vortices with nonzero-mass cores. Noticeably, the latter are found to exhibit an evident Lorentz-like form since, in the presence of vortex cores occupied by a second species, the vortex-motion equations are equivalent to those of a pair of massive charges acted by a transverse magnetic field. With negligible fractions of the minority component, one recovers the Helmholtz-Kirchhoff equations for planar pointlike vortices [42].

The outline of the manuscript is the following: in Sec. II, we present an analytical model for the dynamics of massive vortices in a confined system which incorporates the effect of the virtual vortices resulting from the boundary condition of vanishing normal velocity. In particular, we derive a formula giving the equilibrium distance distinguishing the motion of precession of two corotating massive vortices. Sec. III is devoted to the presentation of the two coupled stationary GPEs which provide a good description of the bosonic binary mixture in the mean-field approximation. In Sec. IV, we show how the presence of massive cores (i.e. species-*b* atoms trapped within species-*a* vortices) affects the equilibrium distance of the pair of corotating vortices. We also show that the interspecies repulsion tends to counterbalance the centrifugal force acting on species-*b* atoms. In Sec. V, we address the angular momenta of the two condensed species and provide analytical formulas that well capture their functional dependence on the number of species-*b* atoms (which, in turn, is directly proportional to the mass of the cores). By means of a suitable change of reference frame, we show that the cores, although following the same motion of precession of the vortices, keep their orientation constant while orbiting. This circumstance witnesses the fact that there is no quantum viscous friction between the two fluids. In Sec. VI, we present an heuristic but effective system of equations that well reproduces the functional dependence of the vortex healing lengths and of the cores' characteristic radius on the number of species-*b* atoms. Eventually, Sec. VII is devoted to concluding remarks.

II. POINTLIKE VORTICES IN A CIRCULAR BOX

In this section, we review some results concerning the dynamics of pointlike vortices and we introduce a model for the dynamics of vortices whose cores host pointlike masses (hence the name *massive* vortices, as opposed to the traditional *massless* vortices).

A. Massless vortices

The Hamiltonian of N pointlike massless vortices in an ideal unbounded fluid is given by [42]

$$H_\infty = (z_1, \dots, z_N) = -\frac{\rho_*}{4\pi} \sum_{i=1}^N \sum_{j \neq i} k_i k_j \ln \frac{|z_i - z_j|}{\lambda} \quad (1)$$

where ρ_* is the fluid planar density, $z_j = x_j + iy_j \in \mathbb{C}$ is the position of the j th vortex in the ambient plane and $k_j = n_j h / m_f$ is its strength ($n_j \in \mathbb{Z}$ and m_f is the fluid particles' mass). In the following, we will specialize our discussion to the case of $N = 2$ vortices.

When one considers bounded systems, Hamiltonian (1) modifies due to the presence of the confining potential. In the case of a box-like potential, the presence of a boundary confining the fluid is accounted for by means of the virtual charge method, i.e. by introducing a suitable configuration of virtual vortices. With this premise in mind, the Hamiltonian of $N = 2$ pointlike massless vortices in an ideal fluid confined in a circular box of radius R reads [43]

$$H = \frac{\rho_*}{4\pi} \left\{ k_1 k_2 \log \frac{|R^2 - z_1 \bar{z}_2|^2}{|R(z_1 - z_2)|^2} + k_1^2 \log \left(1 - \frac{|z_1|^2}{R^2} \right) + k_2^2 \log \left(1 - \frac{|z_2|^2}{R^2} \right) \right\}. \quad (2)$$

In this framework, the coordinates of each vortex constitute a pair of canonically conjugate variables, and motion equations can be obtained by means of the Poisson Brackets

$$\{F, G\} = \frac{1}{\rho_* k_j} \sum_{j=1}^2 \left[\frac{\partial F}{\partial x_j} \frac{\partial G}{\partial y_j} - \frac{\partial G}{\partial x_j} \frac{\partial F}{\partial y_j} \right]$$

involving, in turn, the canonical brackets $\{x_i, y_j\} = \delta_{i,j} / (\rho_* k_j)$ (see for example [44]).

B. Massive vortices

If one wants to introduce into the model the fact that the vortex cores host point masses, it is convenient to move to the Lagrangian formalism, where the presence of massive cores can be taken into account as follows

$$L = \sum_{j=1}^2 \left[\frac{m_j}{2} (\dot{x}_j^2 + \dot{y}_j^2) + \frac{k_j \rho_*}{2} (y_j \dot{x}_j - x_j \dot{y}_j) \right] - H, \quad (3)$$

an expression where m_j represents the pointlike mass hosted by the j th vortex core and where $\dot{q}_j := dq/dt$ (with $q = x, y$). As is well known, the dynamics of the vortex cores is generated by the Euler-Lagrange equations which, in the special but interesting case of two equal vortices $k_1 = k_2 = k$, whose cores host two equal masses $m_1 = m_2 = m$, takes the form

$$m \ddot{\vec{r}}_j = k \rho_* \vec{u}_3 \wedge \dot{\vec{r}}_j + \rho_* \frac{k^2}{2\pi} \left[\frac{\vec{r}_j - \vec{r}_i}{|\vec{r}_j - \vec{r}_i|^2} + \frac{\vec{r}_j}{R^2 - r_j^2} + \frac{R^2 \vec{r}_i - r_i^2 \vec{r}_j}{R^4 - 2R^2 \vec{r}_i \vec{r}_j + r_i^2 r_j^2} \right]$$

for $i, j \in \{1, 2\}$ and $i \neq j$.

The resulting system of 4 differential equations admits a notable solution,

$$\begin{aligned} x_1(t) &= \frac{d}{2} \cos(\Omega t), & y_1(t) &= \frac{d}{2} \sin(\Omega t) \\ x_2(t) &= \frac{d}{2} \cos(\Omega t + \pi), & y_2(t) &= \frac{d}{2} \sin(\Omega t + \pi), \end{aligned}$$

provided that the two vortices are placed symmetrically with respect to the box-trap center and that their distance d and the angular frequency Ω marking their motion of precession fulfill equation

$$\begin{aligned} \frac{\pi d^6 \Omega (k \rho_* - m \Omega) + 3 d^4 k^2 \rho_*}{d - 2R} = \\ - \frac{16 \pi d^2 R^4 \Omega (m \Omega - k \rho_*) + 16 k^2 \rho_* R^4}{d - 2R} \end{aligned} \quad (4)$$

As expected, equation (4) shows a pathology when $d \rightarrow 2R$, meaning that the vortex pair is approaching the circular-box boundary. Moreover, in the limit of infinite box radius ($R \rightarrow +\infty$), one can retain only those terms $\propto R^4$ and the relation $d(\Omega)$ can be expressed in closed form, i.e.:

$$d = k \sqrt{\frac{\rho_*}{\pi}} \frac{1}{\sqrt{k \rho_* \Omega - m \Omega^2}}. \quad (5)$$

In Sec. IV A, the equilibrium distance d predicted by equation (4) and relevant to two equal pointlike massive vortices in a circular box will be compared to the one obtained by numerically solving two coupled stationary GPEs.

III. THE BOSONIC MIXTURE

We consider a bosonic mixture of ^{23}Na and ^{39}K [45, 46]. Each atomic species is characterized by an order parameter, φ_a and φ_b respectively. In a mean-field treatment of the problem, we assume that the system is effectively quasi-2D, as a result of a strong confinement along the z -direction. Because of this, it can be effectively modeled by the following two stationary Gross-Pitaevskii equations

$$\begin{aligned} -\frac{\hbar^2}{2m_a} \left[\frac{\partial^2}{\partial x^2} + \frac{\partial^2}{\partial y^2} \right] \psi_a + \frac{g_a N_a}{\ell_z} |\psi_a|^2 \psi_a \\ + \frac{g_{ab} N_b}{\ell_z} |\psi_b|^2 \psi_a + V_{ext,a} \psi_a = \mu_a \psi_a \\ -\frac{\hbar^2}{2m_b} \left[\frac{\partial^2}{\partial x^2} + \frac{\partial^2}{\partial y^2} \right] \psi_b + \frac{g_b N_b}{\ell_z} |\psi_b|^2 \psi_b \end{aligned}$$

$$+ \frac{g_{ab} N_a}{\ell_z} |\psi_a|^2 \psi_b + V_{ext,b} \psi_b = \mu_b \psi_b \quad (6)$$

where N_a (N_b) corresponds to the number of species- a (species- b) atoms, $g_c = 4\pi\hbar^2 a_c/m_c$, with $c = a, b$ are the intraspecies interaction strengths and $g_{ab} = 2\pi\hbar^2 a_{ab}/m_{ab}$ is the interspecies coupling. Notice that m_a (m_b) is the atomic mass of sodium (potassium), while $m_{ab} = (m_a^{-1} + m_b^{-1})^{-1}$ is their reduced mass; similarly a_a and a_b are the intraspecies scattering lengths, while a_{ab} is the interspecies scattering length. Parameter ℓ_z is the effective thickness of the disklike box trap and functions ψ_a and ψ_b are normalized to 1, in such a way that $\varphi_a = \sqrt{N_a} \psi_a$ and $\varphi_b = \sqrt{N_b} \psi_b$ are, respectively, normalized to N_a and N_b .

Vortical solutions of equations (6) are found by moving to a frame rotating with angular velocity Ω (this corresponds to adding the term $-\Omega \hat{L}_z$ to the Hamiltonian, where \hat{L}_z is the operator associated to the third component of the angular momentum) and then employing the imaginary-time method [47, 48]. The starting condition for the imaginary-time dynamics is such that species- a hosts a vortex pair while species- b is localized (two narrow Gaussian distributions) at the vortex cores. As the fictitious dynamics advances, the position of the vortices cores, their healing length, together with the spatial distribution of species- b atoms is iteratively refined, until convergence is reached.

IV. MASSIVE VORTEX PAIRS IN A BINARY MIXTURE OF BECS

Eigensystem (6) was solved sweeping model parameter N_b , the number of species- b atoms, which constitute the massive cores of species- a vortices. As explained in Sec. III, a suitable ansatz for the starting condition of the imaginary-time dynamics was chosen. In the whole range of N_b that we explored (i.e. $N_b \in [5, 1000]$), our numerical simulations [49] converged to a stationary state of the type illustrated in Fig. 1. Basically, condensate a is highly confined by the box-like potential (whose radius is $R = 50 \mu\text{m}$) and it is marked by the presence of two corotating vortices. The latter are symmetrically positioned with respect to center of the trap, they are such that $|\psi_a|^2$ goes to zero in their cores' centers and feature a quantized circulation. On the other hand, condensate b occupies the vortex cores which, in turn, constitute an effective double-well potential for species- b atoms [41].

One can gain a further insight into the discussed eigensolution by computing the mass current density

$$\vec{J}_c = -\frac{i\hbar}{2} (\psi_c^* \nabla \psi_c - \psi_c \nabla \psi_c^*) \quad (7)$$

(with $c = a, b$) which also corresponds to the momentum-per-particle distribution. As illustrated in the second row

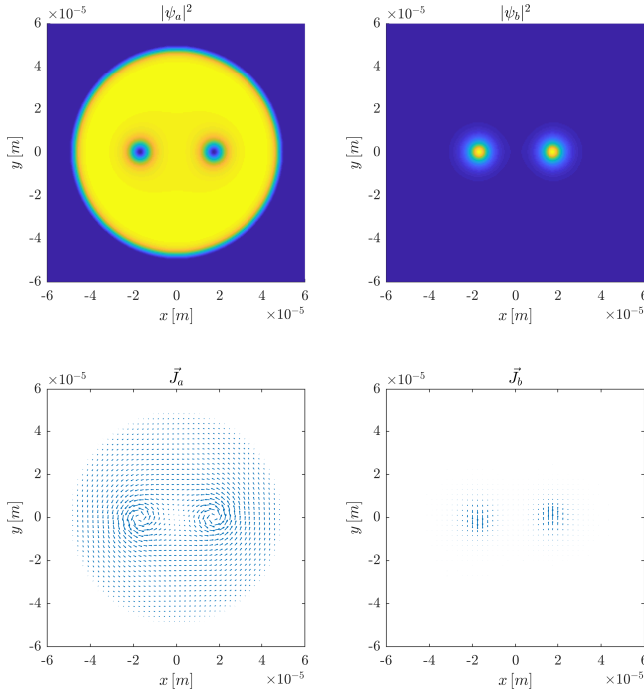


FIG. 1. Typical minimum-energy solution of eigensystem (6). First (second) row corresponds to the square moduli [mass current density (see formula 7)] of the eigensolutions. In the first row, yellow (blue) is associated to large (zero) values of $|\psi|^2$. Left (right) column corresponds to species a (b). The following parameters have been used: $N_a = 5 \cdot 10^4$, $N_b = 10^3$, $\Omega = 5$ rad/s, $R = 50$ μm , $m_a = 3.82 \cdot 10^{-26}$ kg, $m_b = 6.48 \cdot 10^{-26}$ kg, $g_a = 52 \cdot (4\pi\hbar^2 a_0)/m_a$, $g_b = 7.6 \cdot (4\pi\hbar^2 a_0)/m_b$, $g_{ab} = 24.2 \cdot (2\pi\hbar^2 a_0)/m_{ab}$, $\ell_z = 2$ μm .

of Fig. 1, both vortices in species a rotate anticlockwise, thus determining a collective motion of precession which is anticlockwise too. As concerns species- b atoms, they are dragged by condensate a and remain bound within the vortex cores thus featuring their same motion of precession around the center of the trap. With reference to the lower right panel of Fig. 1, one can appreciate that the left (right) peak of $|\psi_b|^2$ is translating downward (upward), i.e. along a direction tangential to the precession orbit.

A. Mass of the cores and equilibrium distance

Increasing the number of species- b atoms (within the investigated range $N_b \in [5, 1000]$), the distance d_{vor} between the vortices' centers *increases*. Similarly, the distance between the two peaks of $|\psi_b|^2$, d_{peak} , increases upon increasing N_b . Fig. 2 shows how the presence of massive cores deforms and displaces the vortices. Notice that the position of the peaks of $|\psi_b|^2$ does not exactly match that of the minima of $|\psi_a|^2$ due to the centrifugal force on species- b atoms and the finite repulsive coupling ($g_{ab} < +\infty$) between the two fluids which, in turn, al-

lows for a non-zero penetration of fluid b into fluid a . Therefore, observables d_{vor} and d_{peak} , which in the analytical model based on pointlike vortices and pointlike massive cores (see Sec. II) collapse on the same variable (d), when estimated from the numerical solution of system (6), despite being closely related, do not necessarily coincide.

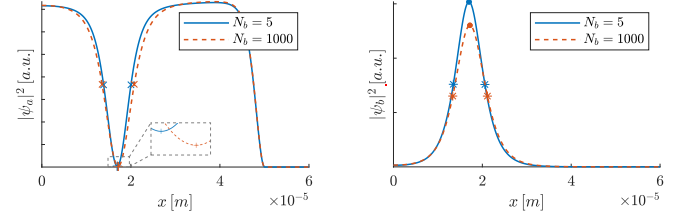


FIG. 2. Profile of the (square modulus of the) minimum-energy solutions of eigensystem (6) along the axis $y = 0$ (we have plotted just the range $x > 0$ because both $|\psi_a|^2$ and $|\psi_b|^2$ are symmetric with respect to $x = 0$) for two different values of N_b . Left panel: the position of markers '+' corresponds to $d_{vor}/2$, while the distance between markers 'x' corresponds to $2\xi_a$. Right panel: the position of markers '.' corresponds to $d_{peak}/2$, while the distance between markers '*' corresponds to $2\sigma_b$. The following parameters have been used: $N_a = 5 \cdot 10^4$, $\Omega = 5$ rad/s, $R = 50$ μm , $m_a = 3.82 \cdot 10^{-26}$ kg, $m_b = 6.48 \cdot 10^{-26}$ kg, $g_a = 52 \cdot (4\pi\hbar^2 a_0)/m_a$, $g_b = 7.6 \cdot (4\pi\hbar^2 a_0)/m_b$, $g_{ab} = 24.2 \cdot (2\pi\hbar^2 a_0)/m_{ab}$, $\ell_z = 2$ μm .

The functional dependence of d_{vor} and d_{peak} [extracted from the numerical solutions of system (6)] on N_b is illustrated in Fig. 3, together with the relation $d(N_b)$, obtained, in turn, by means of substitutions

$$k = \frac{\hbar}{m_a}, \quad \rho_* = \frac{N_a m_a}{\pi R^2}, \quad m = \frac{N_b m_b}{2} \quad (8)$$

into equation (4). Relations (8) allow one to match the analytical model (4) based on pointlike vortices and pointlike massive cores with the actual parameters used to model the quantum fluids within the mean-field approach [see system (6)].

The agreement between the analytical prevision (yellow dotted line) and numerical results (blue solid and red dashed lines) is remarkably good, both qualitatively (same quasi-linear functional dependence on N_b) and quantitatively (offset $< 2\%$). Moreover, we would like to mention that numerical results (namely, the slope and the vertical shift of the corresponding lines of Fig. 3) can be shown to further approach the analytical prevision upon increasing N_a and/or diminishing g_b , two changes that result in narrower cores and, therefore, in a scenario where equation (4), based on the pointlike approximation of vortices and massive cores, reliably describes the mixture vortex state.

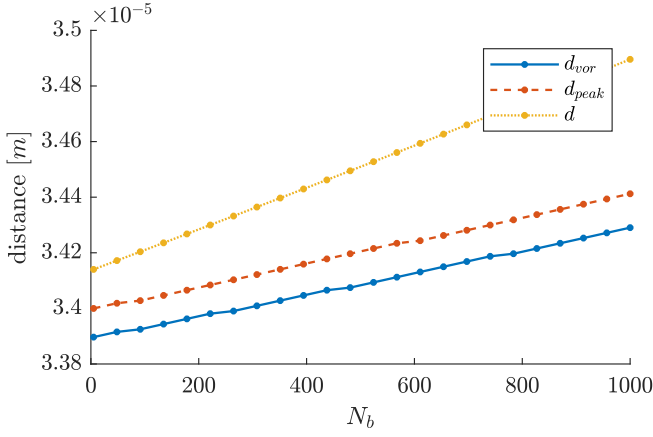


FIG. 3. Equilibrium distance: comparison between numerical (d_{vor} and d_{peak}) and analytical (d) results. The following parameters have been used: $N_a = 5 \cdot 10^4$, $N_b \in [5, 1000]$, $\Omega = 5$ rad/s, $R = 50$ μm , $m_a = 3.82 \cdot 10^{-26}$ kg, $m_b = 6.48 \cdot 10^{-26}$ kg, $g_a = 52 \cdot (4\pi\hbar^2 a_0)/m_a$, $g_b = 7.6 \cdot (4\pi\hbar^2 a_0)/m_b$, $g_{ab} = 24.2 \cdot (2\pi\hbar^2 a_0)/m_{ab}$, $\ell_z = 2$ μm .

B. Competition between centrifugal force and interspecies repulsion

As already mentioned, d_{peak} , although closely related to d_{vor} , is always slightly bigger than the latter. The motion of precession of the vortices around the center of the trap is responsible, in fact, for a centrifugal force on species- b atoms which are, therefore, pushed outwards. This tendency is only partially opposed by the repulsive interaction between the two quantum fluids and it is the competition between these two forces what determines the exact values of d_{vor} and d_{peak} . Increasing g_{ab} , fluid a gets more impenetrable to species- b atoms, which therefore prove to be more tightly bound within the valleys of $|\psi_a|^2$. As a result of this increased reaction to the centrifugal force, the difference $d_{peak} - d_{vor}$ is remarkably smaller, as illustrated in Fig. 4 (where g_{ab} has been set 2.5 times bigger than the value used for Fig. 3).

V. ANGULAR MOMENTUM OF VORTICES AND CORES

This section is devoted to the analysis of the angular momentum of each condensed species, an investigation that can offer a deeper insight into the Physics of the system. In particular, we show that the two massive cores (made of species- b atoms) *orbit* around the center of the trap, being dragged by the motion of precession of the vortices. Nevertheless, they do not *rotate*, i.e. their orientation remains constant while they revolve.

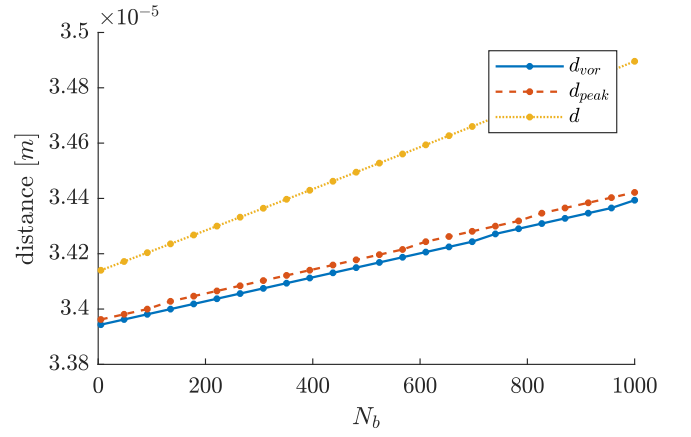


FIG. 4. Equilibrium distance: comparison between numerical (d_{vor} and d_{peak}) and analytical (d) results. For these simulations, parameter g_{ab} is 2.5 times bigger than the one used for Fig. 3, all the others being unchanged.

A. Angular momentum of condensate a

The angular momentum (per particle, in units of \hbar) of condensate a can be computed as

$$\frac{\langle L_{z,a} \rangle}{N_a \hbar} = -i \int \psi_a^* \left(x \frac{\partial}{\partial y} - y \frac{\partial}{\partial x} \right) \psi_a dx dy \quad (9)$$

This quantity can be evaluated numerically from the solution of system (6).

On the other hand, it can also be estimated by means of a fully-analytical approach. Along the same lines discussed in Ref. [50] (where the authors investigated the case of *harmonic* confinement), in fact, it is possible to derive formula

$$\frac{\tilde{L}_{z,a}}{N_a \hbar} = 2 \int_{r_{vor}}^R 2\pi r \frac{1}{\pi R^2} dr = 2 \left[1 - \left(\frac{r_{vor}}{R} \right)^2 \right], \quad (10)$$

where $r_{vor} := d_{vor}/2$ constitutes the orbit radius.

As shown in Fig. 5, formula (10) well fits the numerical data obtained by means of formula (9), the mismatch being $< 0.8\%$. In this regard, it can be shown that the fitting accuracy further increases if one increases N_a and/or decreases g_b , because, in this case, the pointlike approximation of vortices and cores gets increasingly valid.

B. Angular momentum of condensate b

The angular momentum (per particle, in units of \hbar) of condensate b can be computed as

$$\frac{\langle L_{z,b} \rangle}{N_b \hbar} = -i \int \psi_b^* \left(x \frac{\partial}{\partial y} - y \frac{\partial}{\partial x} \right) \psi_b dx dy, \quad (11)$$

a quantity that can be evaluated numerically on the basis of the solution of system (6).

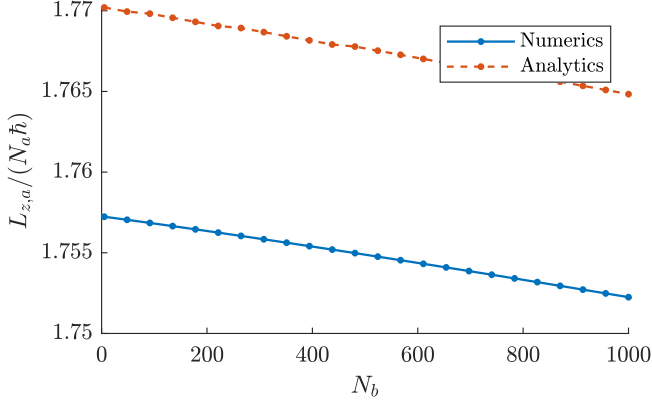


FIG. 5. Angular momentum (per particle, in units of \hbar) of condensate a : comparison between numerical [see formula (9)] and analytical [see formula (10)] results. The following parameters have been used: $N_a = 5 \cdot 10^4$, $N_b \in [5, 1000]$, $\Omega = 5$ rad/s, $R = 50 \mu\text{m}$, $m_a = 3.82 \cdot 10^{-26}$ kg, $m_b = 6.48 \cdot 10^{-26}$ kg, $g_a = 52 \cdot (4\pi\hbar^2 a_0)/m_a$, $g_b = 7.6 \cdot (4\pi\hbar^2 a_0)/m_b$, $g_{ab} = 24.2 \cdot (2\pi\hbar^2 a_0)/m_{ab}$, $\ell_z = 2 \mu\text{m}$.

As already mentioned, the two species- b cores orbit around the center of the trap but they do not rotate around their own centers of mass. To prove this statement, we proceed along two different lines.

a. Mass current density in the rotating frame. In the lab frame, it is possible to compute the mass current density \vec{J}_b associated to ψ_b [see formula (7)]. The corresponding vector field is illustrated in the bottom right panel of Fig. 1. It is clear that the left (right) core is moving downward (upward), dragged by the anticlockwise motion of precession of the vortices. Due to the characteristic magnitude of $|\vec{J}_b|$, this plot does not allow one to understand whether the cores change their orientation or not along their orbit around the center of the trap. To circumvent this limitation, we have computed the species- b mass current density in a frame rotating with the same angular velocity Ω distinguishing the motion of precession of the vortices. More specifically, the species- b mass current density in the rotating frame, $\vec{J}_{b,rot}$, is obtained starting from the one defined by formula (7), moving to the associated velocity field

$$\vec{v}_b = \frac{\vec{J}_b}{m_b |\psi_b|^2},$$

where it is possible to enact the transformation $\vec{v}_b \rightarrow \vec{v}_{b,rot} = \vec{v}_b - \vec{V}$ [where $\vec{V} = \vec{\Omega} \wedge \vec{r} = (\Omega \vec{z}) \wedge \vec{r}$ is the velocity vector field associated to the relative rotation of the two frames] and then coming back to the mass current density vector field

$$\vec{J}_{b,rot} = m_b |\psi_b|^2 \vec{v}_{b,rot} \quad (12)$$

Notice, in this regard, that the lab frame xOy and the rotating frame $x'O'y'$ are such that $O \equiv O' \quad \forall t$, while $x \equiv x'$ and $y \equiv y'$ at $t = 0$. Notice also that, at $t = 0$,

$|\psi_b|^2 \equiv |\psi'_b|^2$, thus justifying its use in formula (12). The result of this procedure is illustrated in the left panel of Fig. 6 which shows that the two species- b cores, when observed from the rotating frame, rotate around their respective centers of mass, with angular velocity $-\Omega$ (the minus sign being due to the *clockwise* direction). On top

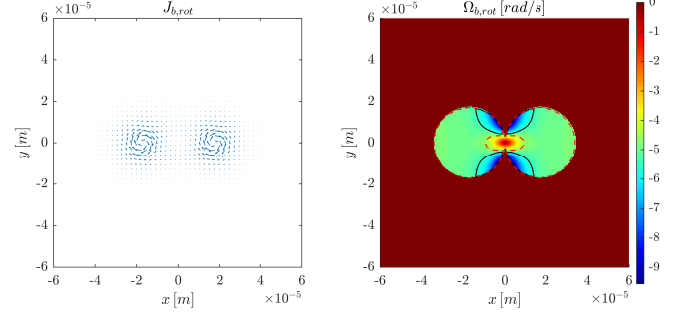


FIG. 6. Left panel: species- b mass current density in the rotating frame [see formula (12) and the relevant explanation]: one can appreciate the two cores rotate *clockwise*. Right panel: species- b local angular velocity, as defined by formula (13); The solid black and red dashed lines correspond to $\tilde{\Omega}_{b,rot} = -5 \pm 0.5$ rad/s and have been drawn to illustrate that the two species- b cores indeed rotate as two (almost) rigid bodies (see discussion in the main text). The following parameters have been used: $N_a = 5 \cdot 10^4$, $N_b = 10^3$, $\Omega = 5$ rad/s, $R = 50 \mu\text{m}$, $m_a = 3.82 \cdot 10^{-26}$ kg, $m_b = 6.48 \cdot 10^{-26}$ kg, $g_a = 52 \cdot (4\pi\hbar^2 a_0)/m_a$, $g_b = 7.6 \cdot (4\pi\hbar^2 a_0)/m_b$, $g_{ab} = 24.2 \cdot (2\pi\hbar^2 a_0)/m_{ab}$, $\ell_z = 2 \mu\text{m}$.

of that, we have evidenced how these two cores rotate almost as if they were rigid bodies, meaning that the (absolute value of the) velocity field $\vec{v}_{b,rot}$ around each center of mass linearly increases with the distance r_C from the respective center of mass [in view of the symmetry of the ground-state configuration depicted in Fig. 1, we refer to the left (right) center of mass when considering the velocity field in the half-plane $x < 0$ ($x > 0$)]. The right panel of Fig. 6 shows the local angular velocity of species- b cores when observed from the rotating frame. This quantity, defined as

$$\tilde{\Omega}_{b,rot}(x, y) = -\frac{|\vec{v}_{b,rot}|}{r_C}, \quad (13)$$

[where r_C is the distance of point (x, y) from the left (right) center of mass when $x < 0$ ($x > 0$)], takes the (almost) constant value ≈ -5 rad/s in the most part of the regions where $|\psi_b|^2$ is non-zero.

In conclusion, we have proved that, in the rotating frame, the two species- b cores rotate around their respective centers of mass with (almost uniform) angular velocity $-\Omega$. This allows us to conclude that they keep their orientation fixed when observed from the lab frame.

b. Analytical estimate of the angular momentum. To corroborate what elucidated in the previous paragraph, we show that the functional dependence of quantity (11) on model parameter N_b can be well fitted by

the semi-analytical model

$$\frac{\tilde{L}_{z,b}}{N_b\hbar} \approx \frac{\tilde{\mathcal{L}}_{O,b}}{N_b\hbar} + \frac{\tilde{\mathcal{S}}_{C_L,b}}{N_b\hbar} + \frac{\tilde{\mathcal{S}}_{C_R,b}}{N_b\hbar} \quad (14)$$

where

$$\frac{\tilde{\mathcal{L}}_{O,b}}{N_b\hbar} = \frac{\Omega}{\hbar} \int m_b |\psi_b|^2 r^2 dx dy \quad (15)$$

and where terms

$$\frac{\tilde{\mathcal{S}}_{C_L,b}}{N_b\hbar} = -\frac{\Omega}{\hbar} \int m_b |\psi_b|^2 \Theta(-x) r_{C_L}^2 dx dy \quad (16)$$

$$\frac{\tilde{\mathcal{S}}_{C_R,b}}{N_b\hbar} = -\frac{\Omega}{\hbar} \int m_b |\psi_b|^2 \Theta(x) r_{C_R}^2 dx dy \quad (17)$$

are introduced to take into account that, in the lab frame, the two species- b cores revolve but keep their orientation fixed [Heaviside functions $\Theta(-x)$ and $\Theta(x)$ allow one to select the left and the right core respectively]. The integrals in expressions (15)-(17) represent three moment of inertia corresponding, respectively, to the anticlockwise revolution of the whole system around the center of the trap O , and to the effective clockwise rotation of the left (right) core around its own center of mass C_L (C_R) [in this regard, $r^2 := x^2 + y^2$, $r_{C_L}^2 := (x - x_{C_L})^2 + (y - y_{C_L})^2$, $r_{C_R}^2 := (x - x_{C_R})^2 + (y - y_{C_R})^2$]. The latter effective motions indeed compensate for the fact that a *pure* motion of revolution [captured by formula (15)] would determine a *change* in the orientation of the cores along the circular orbit. Figure 7 shows a very good agreement between formula (11) and model (14), the error being always $< 4\%$.

We conclude this section by observing that the interspecies repulsive coupling is the interaction underlining the dragging of species- b cores by species- a vortices, which therefore exhibit the same motion of precession. Also, one could expect to observe some kind of quantum viscous friction between the two fluids, i.e. that species- a vortices could put species- b cores into rotation (around their own centers of mass). This was not observed in our numerical experiments, possibly because we employed values of g_{ab} high enough to determine a sufficiently small overlap between ψ_a and ψ_b , a circumstance which, in turn, could prevent the vortices from tangentially dragging the massive cores that they host. This aspect will be further investigated in a future work.

VI. VORTEX HEALING LENGTHS AND SIZE OF THE MASSIVE CORES

The presence of species- b massive cores within species- a vortices affects the healing length of the latter. The intraspecies repulsive interaction, in fact, tends to enlarge the cores which, in turn, tend to swell (from the inside)

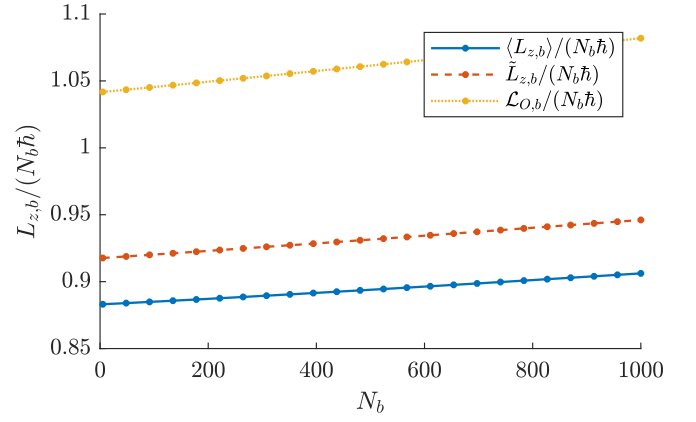


FIG. 7. Angular momentum (per particle, in units of \hbar) of condensate b : comparison between numerical [solid blue line, associated to formula (11)] and semi-analytical [red dashed line, corresponding to formula (14)] results [the yellow dotted line, associated to formula (15) represents the angular momentum of the system if its motion was a pure revolution around the center of the trap O]. The following parameters have been used: $N_a = 5 \cdot 10^4$, $N_b \in [5, 1000]$, $\Omega = 5$ rad/s, $R = 50 \mu\text{m}$, $m_a = 3.82 \cdot 10^{-26}$ kg, $m_b = 6.48 \cdot 10^{-26}$ kg, $g_a = 52 \cdot (4\pi\hbar^2 a_0)/m_a$, $g_b = 7.6 \cdot (4\pi\hbar^2 a_0)/m_b$, $g_{ab} = 24.2 \cdot (2\pi\hbar^2 a_0)/m_{ab}$, $\ell_z = 2 \mu\text{m}$.

the vortices' profile because of the interspecies repulsive coupling. Flipping the perspective, the cores' expansion is dammed by the species- a fluid, which plays the role of an effective confining potential for species- b atoms.

In the attempt to estimate the equilibrium healing length ξ_a of species- a vortices and the equilibrium characteristic size of species- b cores, σ_b , we present the following heuristic equations

$$\begin{aligned} \frac{\hbar^2}{2m_a} \frac{1}{\xi_a^2} &= +g_a n_a - g_{ab} n_a n_b \pi (\sigma_b^2 - \xi_a^2) \ell_z \\ \frac{\hbar^2}{2m_b} \frac{1}{\sigma_b^2} &= -g_b n_b + g_{ab} n_a n_b \pi (\sigma_b^2 - \xi_a^2) \ell_z \end{aligned} \quad (18)$$

where

$$n_a = \frac{N_a}{\pi r_{box}^2 \ell_z}, \quad n_b = \frac{N_b/2}{\pi \sigma_b^2 \ell_z}.$$

Notice that the the first equation of system (18) reduces, in the case of no interspecies interaction, to

$$\xi_{a,0} = \sqrt{\frac{\hbar^2}{2m_a g_a n_a}},$$

the well-known formula derived in the context of single-species vortices [51]. Similarly, the second equation, if $g_{ab} = 0$, gets structurally similar to formula

$$\sigma_{b,0} = \sqrt{\frac{\hbar^2}{2m_b |g_b| n_{b,0}}},$$

giving the characteristic size of a soliton in the case of attractive interactions [51] (of course, in this context, $n_{b,0}$ represents the central density). The extra term $g_{ab}n_a n_b \pi(\sigma_b^2 - \xi_a^2)\ell_z$ is introduced to take into account the interspecies repulsion, an interaction that manifests only in those regions where ψ_a and ψ_b overlap, i.e. only in the two annuli centered in the vortices' centers and whose outer and inner radii are σ_b and ξ_a respectively.

In order to compare the previsions provided by equations (18) with the measurements extracted from the numerical solutions of system (6), one has to give the operational definition of “vortex healing length” and “core characteristic size”. From the numerical side, with reference to Fig. 2, we agree to measure the half width at half maximum of the valley of $|\psi_a|^2$, λ_a , and the half width at half maximum of the peak of $|\psi_b|^2$, λ_b . From the analytical side, the estimates of quantities λ_a and λ_b are given by the solutions of system (18), ξ_a and σ_b , multiplied by two suitable constant conversion factors, 1.30 and 1.15 respectively, which are determined from their numerical counterpart in the case $N_b = 1$, that means in a scenario where species- b cores have a negligible impact on species- a vortices.

As illustrated in Fig. 8, equations (18) well capture the functional dependence of λ_a and of λ_b on N_b .

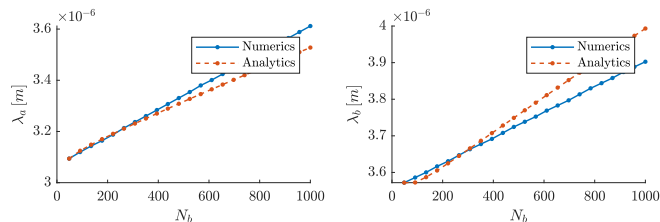


FIG. 8. Left (right) panel: comparison between the numerically- determined and the analytically- estimated half width half maximum, λ_a , of species- a vortices (of species- b cores, λ_b). The following parameters have been used: $N_a = 5 \cdot 10^4$, $N_b \in [1, 1000]$, $\Omega = 5$ rad/s, $R = 50$ μ m, $m_a = 3.82 \cdot 10^{-26}$ kg, $m_b = 6.48 \cdot 10^{-26}$ kg, $g_a = 52 \cdot (4\pi\hbar^2 a_0)/m_a$, $g_b = 7.6 \cdot (4\pi\hbar^2 a_0)/m_b$, $g_{ab} = 24.2 \cdot (2\pi\hbar^2 a_0)/m_{ab}$, $\ell_z = 2$ μ m.

VII. CONCLUDING REMARKS

In this work, we have investigated a notable class of configurations exhibited by a bosonic binary mixture

loaded in a box-like circular trap, namely, minimum-energy states where species- b atoms are trapped within the vortex cores of species- a fluid. Both within a fully-analytical framework and by means of a systematic analysis of the numerical solutions of the associated two coupled GPEs, we have shown that the presence of massive cores alters the equilibrium distance distinguishing the motion of precession of the vortex pair. Interestingly, for the considered choices of model parameters (repulsive intra- and interspecies interactions such that, in the homogeneous case, the miscibility condition $g_{ab} < \sqrt{g_a g_b}$ is not met) the dynamical mean-field picture of the mixture has been shown to reduce to much simpler effective equations exhibiting an evident Lorentz-like magnetic form, where massive vortices play the role of massive charges confined on a plane and subject to a magnetic field. Species- b cores, in turn, are dragged by fluid a and thus follow their same motion of precession around the trap center; nevertheless, while orbiting, they keep their orientation constant, meaning that there is no quantum viscous friction between the two fluids. We have also derived, in the context of the Thomas-Fermi approximation, a simple formula to estimate the angular momentum of condensate a and we have shown, by means of a suitable change of reference frame, that species- b cores effectively behave as two rigid bodies. Eventually, we have introduced a system of heuristic but effective equations to estimate the characteristic size of vortices and cores hosted therein.

ACKNOWLEDGEMENTS

The authors wish to thank M. Pi, A. Gallemí and Y. Bidasyuk for their valuable help in setting up the numerical simulations. M. G. and R. M. acknowledge financial support from the Spanish MINECO and Fondo Europeo de Desarrollo Regional (FEDER, EU) under Grant No. FIS2017-87801-P, and from Generalitat de Catalunya Grant No. 2017SGR533.

[1] L. Onsager, *Il Nuovo Cimento* (1943-1954) **6**, 279 (1949).
[2] L. M. Pismen and L. M. Pismen, *Vortices in nonlinear fields: from liquid crystals to superfluids, from non-equilibrium patterns to cosmic strings*, Vol. 100 (Oxford University Press, Oxford, UK, 1999).
[3] R. P. Feynman, in *Progress in low temperature physics*, Vol. 1 (Elsevier, 1955) pp. 17–53.

[4] R. J. Donnelly, *Quantized vortices in helium II*, Vol. 2 (Cambridge University Press, 1991).
[5] M. Brambilla, L. A. Lugiato, V. Penna, F. Prati, C. Tamm, and C. O. Weiss, *Phys. Rev. A* **43**, 5114 (1991).
[6] I. Carusotto and C. Ciuti, *Rev. Mod. Phys.* **85**, 299 (2013).

- [7] G. Blatter, M. V. Feigel'man, V. B. Geshkenbein, A. I. Larkin, and V. M. Vinokur, *Rev. Mod. Phys.* **66**, 1125 (1994).
- [8] R. P. Huebener, *Magnetic flux structures in superconductors: extended reprint of a classic text*, Vol. 6 (Springer Science & Business Media, 2013).
- [9] Vortex dynamics and quantum effects in Josephson junction arrays are reviewed in the Proceedings of the ICTP Workshop on Josephson Junction Arrays, edited by H.A. Cardeira and S.R. Shenoy [*Physica B* 222 (1996) 336], .
- [10] R. Fazio and H. Van Der Zant, *Physics Reports* **355**, 235 (2001).
- [11] C. F. Barenghi, R. J. Donnelly, and W. Vinen, *Quantized vortex dynamics and superfluid turbulence*, Vol. 571 (Springer Science & Business Media, 2001).
- [12] J. M. Kosterlitz and D. J. Thouless, *Journal of Physics C: Solid State Physics* **6**, 1181 (1973).
- [13] R. Y. Chiao, A. Hansen, and A. A. Moulthrop, *Phys. Rev. Lett.* **54**, 1339 (1985).
- [14] A. L. Fetter, *Phys. Rev.* **162**, 143 (1967).
- [15] M. Rasetti and T. Regge, *Physica A: Statistical Mechanics and its Applications* **80**, 217 (1975).
- [16] V. Penna, M. Rasetti, and M. Spera, *Contemporary Mathematics* **219**, 173 (1998).
- [17] A. L. Fetter, *Rev. Mod. Phys.* **81**, 647 (2009).
- [18] R. Dum, J. I. Cirac, M. Lewenstein, and P. Zoller, *Phys. Rev. Lett.* **80**, 2972 (1998).
- [19] D. Butts and D. Rokhsar, *Nature* **397**, 327 (1999).
- [20] F. Dalfovo and S. Stringari, *Physical Review A* **53**, 2477 (1996).
- [21] L. Pismen and J. Rubinstein, *Physica D: Nonlinear Phenomena* **47**, 353 (1991).
- [22] M. Cozzini and S. Stringari, *Phys. Rev. A* **67**, 041602 (2003).
- [23] Y. Castin and R. Dum, *The European Physical Journal D - Atomic, Molecular, Optical and Plasma Physics* **7**, 399 (1999).
- [24] M. R. Matthews, B. P. Anderson, P. Haljan, D. Hall, C. Wieman, and E. A. Cornell, *Physical Review Letters* **83**, 2498 (1999).
- [25] A. Recati, F. Zambelli, and S. Stringari, *Phys. Rev. Lett.* **86**, 377 (2001).
- [26] S. Sinha and Y. Castin, *Phys. Rev. Lett.* **87**, 190402 (2001).
- [27] K. W. Madison, F. Chevy, V. Bretin, and J. Dalibard, *Phys. Rev. Lett.* **86**, 4443 (2001).
- [28] R. Onofrio, C. Raman, J. M. Vogels, J. R. Abo-Shaeer, A. P. Chikkatur, and W. Ketterle, *Phys. Rev. Lett.* **85**, 2228 (2000).
- [29] D. R. Scherer, C. N. Weiler, T. W. Neely, and B. P. Anderson, *Phys. Rev. Lett.* **98**, 110402 (2007).
- [30] P. G. Drazin and R. S. Johnson, *Solitons: an introduction*, Vol. 2 (Cambridge university press, Cambridge, UK, 1989).
- [31] S. Burger, L. D. Carr, P. Öhberg, K. Sengstock, and A. Sanpera, *Phys. Rev. A* **65**, 043611 (2002).
- [32] D. Frantzeskakis, *Journal of Physics A: Mathematical and Theoretical* **43**, 213001 (2010).
- [33] C. Becker, S. Stellmer, P. Soltan-Panahi, S. Dörscher, M. Baumert, E.-M. Richter, J. Kronjäger, K. Bongs, and K. Sengstock, *Nature Physics* **4**, 496 (2008).
- [34] C. Hamner, J. Chang, P. Engels, and M. Hoefer, *Physical review letters* **106**, 065302 (2011).
- [35] S. Middelkamp, J. Chang, C. Hamner, R. Carretero-González, P. Kevrekidis, V. Achilleos, D. Frantzeskakis, P. Schmelcher, and P. Engels, *Physics Letters A* **375**, 642 (2011).
- [36] T. Busch and J. R. Anglin, *Phys. Rev. Lett.* **87**, 010401 (2001).
- [37] V. M. Pérez-García and J. B. Beitia, *Phys. Rev. A* **72**, 033620 (2005).
- [38] K. J. H. Law, P. G. Kevrekidis, and L. S. Tuckerman, *Phys. Rev. Lett.* **105**, 160405 (2010).
- [39] K. Mukherjee, S. Mistakidis, P. Kevrekidis, and P. Schmelcher, *arXiv preprint arXiv:1904.06208* (2019).
- [40] E. G. Charalampidis, P. G. Kevrekidis, D. J. Frantzeskakis, and B. A. Malomed, *Phys. Rev. E* **94**, 022207 (2016).
- [41] M. Pola, J. Stockhofe, P. Schmelcher, and P. G. Kevrekidis, *Phys. Rev. A* **86**, 053601 (2012).
- [42] P. G. Saffman, *Vortex dynamics* (Cambridge university press, Cambridge, UK, 1992).
- [43] V. Penna, in *Quantized Vortex Dynamics and Superfluid Turbulence*, edited by C.F. Barenghi, R.J. Donnelly, and W.F. vinen (Springer-Verlag, Berlin 2001), pp 445-452, .
- [44] V. Penna, *Phys. Rev. B* **59**, 7127 (1999).
- [45] T. A. Schulze, T. Hartmann, K. K. Voges, M. W. Gempe, E. Tiemann, A. Zenesini, and S. Ospelkaus, *Phys. Rev. A* **97**, 023623 (2018).
- [46] A. Richaud, A. Zenesini, and V. Penna, *Sci. Rep.* **9**, 6908 (2019).
- [47] F. Coppens, F. Ancilotto, M. Barranco, N. Halberstadt, and M. Pi, *Physical Chemistry Chemical Physics* **19**, 24805 (2017).
- [48] A. Gallemí, L. P. Pitaevskii, S. Stringari, and A. Recati, *Phys. Rev. A* **97**, 063615 (2018).
- [49] Computational resources provided by HPC@POLITO (<http://www.hpc.polito.it>), .
- [50] M. Guilleumas and R. Graham, *Phys. Rev. A* **64**, 033607 (2001).
- [51] L. Pitaevskii and S. Stringari, *Bose-Einstein condensation and superfluidity*, Vol. 164 (Oxford University Press, 2016).